AGU PUBLICATIONS

JGR

Journal of Geophysical Research: Space Physics

RESEARCH ARTICLE
10.1002/2016JA022633

Key Points:
- First observation of shrinking equatorial plasma bubbles
- The shrink speeds over the dip equator are different from the bottomside vertical drifts
- Newly identified decay phase showing that the equatorial plasma bubbles can decay before sunrise

Correspondence to:
V. L. Narayanan,
narayananvlwins@gmail.com;
narayananvl@iisermohali.ac.in

Citation:
Narayanan, V. L., S. Gurubaran, K. Shiokawa, and K. Emperumal (2016), Shrinking equatorial plasma bubbles, *J. Geophys. Res. Space Physics*, *121*, doi:10.1002/2016JA022633.

Received 29 FEB 2016
Accepted 28 JUN 2016
Accepted article online 2 JUL 2016

Shrinking equatorial plasma bubbles

V. L. Narayanan[1], S. Gurubaran[2], K. Shiokawa[3], and K. Emperumal[4]

[1]Indian Institute of Science Education and Research Mohali, Mohali, India, [2]Indian Institute of Geomagnetism, Mumbai, India, [3]Institute for Space-Earth Environmental Research, Nagoya University, Nagoya, Japan, [4]Equatorial Geophysical Research Laboratory, Indian Institute of Geomagnetism, Tirunelveli, India

Abstract The formation of equatorial plasma bubbles (EPBs) associated with spread *F* irregularities are fairly common phenomenon in the postsunset equatorial ionosphere. These bubbles grow as a result of eastward polarization electric field resulting in upward $E \times B$ drift over the dip equator. As they grow they are also mapped to low latitudes along magnetic field lines. The EPBs are often observed as airglow depletions in the images of OI 630 nm emission. On occasions the growth of the features over the dip equator is observed as poleward extensions of the depletions in all-sky images obtained from low latitudes. Herein, we present interesting observations of decrease in the latitudinal extent of the EPBs corresponding to a reduction in their apex altitudes over the dip equator. Such observations indicate that these bubbles not only grow but also shrink on occasions. These are the first observations of shrinking EPBs. The observations discussed in this work are based on all-sky airglow imaging observations of OI 630.0 nm emission made from Panhala (11.1°N dip latitude). In addition, ionosonde observations made from dip equatorial site Tirunelveli (1.1°N dip latitude) are used to understand the phenomenon better. The analysis indicates that the speed of shrinking occurring in the topside is different from the bottomside vertical drifts. When the EPBs shrink, they might decay before sunrise hours.

1. Introduction

Equatorial plasma bubbles (EPBs) are large-scale plasma depletions that originate over the dip equator in the nighttime *F* region ionosphere due to the generalized Rayleigh-Taylor instability process. The instability is triggered by perturbations in the bottomside *F* region [*Kelley et al.*, 1981; *McClure et al.*, 1998; *Sekar et al.*, 2001; *Abdu et al.*, 2009, 2015; *Narayanan et al.*, 2012] when the background ionosphere in the post sunset hours is favorable for growth of the instability [*Abdu et al.*, 1983; *Jayachandran et al.*, 1993; *Fejer et al.*, 1999]. They often grow to the topside ionospheric altitudes within few tens of minutes [*Sultan*, 1996; *Sidorova and Filippov*, 2014; *Patra et al.*, 2014]. As they rise in altitude, the depletions are mapped to low latitudes along the geomagnetic field lines [*Rohrbaugh et al.*, 1989]. The numerical simulations by *Krall et al.* [2010a] address issue of maximum growth of EPBs and show that EPBs grow up to the altitudes where the field-line-integrated ion mass density within the EPBs is equal to that of the surroundings. This reflects the earlier belief that the growth of the EPBs stops when the field-line-integrated electron densities within and outside the EPBs are same [*Mendillo et al.*, 2005]. Another possibility to stop the growth of the EPBs might be the decay of the polarization electric field within the depletions. When the polarization field decays, the $E \times B$ drift that lifts up the depleted region stops and the growth of the bubbles will cease.

The intensity of airglow emissions arising in the thermospheric altitudes, particularly that of OI 630 nm line, is proportional to the electron density, and hence, these EPBs are seen as depletions in the airglow intensity. Therefore, imaging observations of OI 630 nm emissions from low latitudes often capture the signature of EPBs and are one of the important measurement methods to study these features [*Rohrbaugh et al.*, 1989; *Makela*, 2006; *Martinis and Mendillo*, 2007; *Narayanan et al.*, 2012; *Shiokawa et al.*, 2015]. In situ observations of EPBs are made with satellite and rocket measurements as well [*Rino et al.*, 1981; *Aggson et al.*, 1992, 1996; *Laakso et al.*, 1994; *McClure et al.*, 1998]. It is well known that the spreading of *F* region traces in nocturnal low-latitude ionograms is due to EPBs [e.g., *Lynn et al.*, 2011; *Narayanan et al.*, 2012, 2014]. The larger EPBs host electron density irregularities from kilometer- to centimeter-scale sizes. The smaller-scale irregularities not only exist within the EPBs but also in the region surrounding them [*Aggson et al.*, 1992]. The small-scale irregularities of few meter-scale sizes are studied with the help of VHF radars [*Woodman and La Hoz*, 1976; *Rao et al.*, 1997; *Saito et al.*, 2008; *Patra et al.*, 2014], while those irregularities with few hundred meter-scale sizes are studied with scintillation measurements [e.g., *Basu et al.*, 1978; *Bhattacharyya et al.*, 2014].

The current understanding is that the small-scale irregularities decay sooner, while the EPBs themselves persist till sunrise as inactive fossil features. This is because cross field plasma diffusion is an extremely slow process to refill depletions with scale sizes of few tens of kilometers [*Burke et al.*, 1979; *Sidorova and Filippov*, 2014]. Since the production decreases with height in the *F* region ionosphere due to the decreasing density, longer periods are required to refill the top portions of the EPBs. Estimations show that it takes a few hours after sunrise to refill depleted flux tubes at altitudes greater than 700 km [*Huang et al.*, 2013; *Sidorova and Filippov*, 2014]. There are many reports on scintillation and EPB measurements in the ionization anomaly crest regions around 15° magnetic latitudes [*Immel et al.*, 2004; *Lee et al.*, 2009; *Candido et al.*, 2011; *Abadi et al.*, 2014]. Only those EPBs that have grown to apex altitudes of 750 km and above over the dip equator can be observed at such latitudes. Further, there are few reports showing the existence of EPBs at magnetic latitudes as large as 30° [*Martinis and Mendillo*, 2007; *Martinis et al.*, 2009; *Otsuka et al.*, 2012]. In these extreme cases the apex altitudes reached by the EPBs over the dip equator penetrate into the plasmasphere and satellite observations of topside He^+ depletions are indeed interpreted as signature of EPBs [*Sidorova*, 2007; *Sidorova and Filippov*, 2014]. The time required to fill those depletions will be on the order of several hours after sunrise. There are few scarce reports on the identification of spread *F*-like features in the sunlit hours [*Dyson*, 1977; *Woodman et al.*, 1985; *Watanabe and Oya*, 1986; *Chau and Woodman*, 2001; *Huang et al.*, 2013]. However, given the amount of EPB observations around EIA crest region, it is unclear why only very few observations show the existence of EPBs after sunrise.

Recent reports based on airglow observations revealed cases in which EPBs disappear due to interaction with traveling ionospheric disturbances (TIDs) [*Otsuka et al.*, 2012; *Shiokawa et al.*, 2015]. The polarization electric fields associated with the TIDs are identified to have caused disappearance of the EPBs. In the study by *Otsuka et al.* [2012], a medium-scale TID was found to feed the ambient plasma into the EPB by inducing $E \times B$ drift. A similar mechanism was proposed by *Shiokawa et al.* [2015] but with a large-scale TID. In the latter case, equatorial spread *F* (ESF) signatures were seen in the ionograms in spite of significant decrease in EPB signature in airglow images at conjugate locations. However, those are special cases wherein the EPBs and TIDs met.

In this work, for the first time, we show that on occasions the whole EPBs collapse or shrink toward the bottomside ionosphere from higher apex altitudes. We use airglow imaging observations of OI 630 nm emissions to identify this phenomenon. Such shrinking was not noticed in earlier observations, and it is important because it appears like a newly identified phase during the decay of EPBs. The EPBs seem to have been pushed back into the bottomside *F* region where they become extinct. This indicates that it is not necessary for all the EPBs to stay till morning hours in order to be refilled. We also make a proposal to explain why only some of the EPBs show such a collapsing behavior.

2. Database

EPBs are frequently observed over Indian region using all-sky imaging observations [*Sinha and Raizada*, 2000; *Mukherjee*, 2003; *Rajesh et al.*, 2010; *Narayanan et al.*, 2012; *Nade et al.*, 2013, 2015; *Sharma et al.*, 2014; *Taori and Sindhya*, 2014]. We utilize all-sky imaging of OI 630 nm emission obtained from Indian station Panhala (16.8°N, 74.1°E geographic, 11.1°N dip latitude) in campaign mode observations during January to March 2008. Detailed information about the instrument, 3 month campaign at Panhala, observation routines, and data analysis methods are discussed in detail in earlier works [*Narayanan et al.*, 2009, 2011, 2013]. The different airglow emissions are observed with the help of interference filters of ~2 nm bandwidths except for OH emission observed with a broadband notch filter. The observations were carried out by manual operation of the imager during these campaigns. A set of images were acquired continuously for a particular airglow emission, and the emissions were selected nearly in a sequence. However, since the instrument has six interference filters to probe both mesospheric and thermospheric airglow lines and was operated manually, the sequence was interrupted often when some interesting events were found to occur in some of the emissions. Therefore, it becomes difficult to use keograms for analysis of the campaign data [*Narayanan et al.*, 2013].

Here we focus on observations during the nights of 4 and 6 January and 3 and 4 February 2008, wherein the EPBs are seen to collapse clearly. The images are unwarped and projected on geographical coordinates following the method described in *Narayanan et al.* [2009]. The magnetic latitudes corresponding to the geographical latitudinal extent covered by the imager field of view are calculated based on International Geomagnetic Reference Field 11 model [*Finlay et al.*, 2010] for 74°E longitude. Note that the magnetic latitudes are not differing by

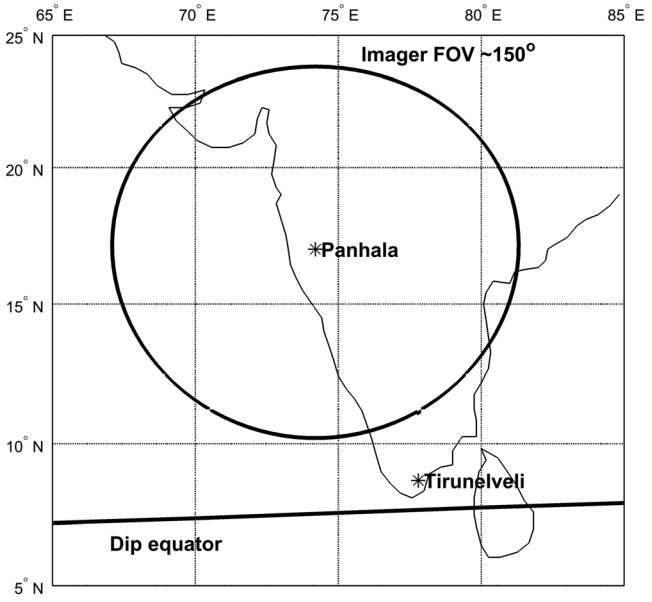

Figure 1. Schematic map showing the observation locations of airglow imager and ionosonde, the area covered by the field of view of imager at 250 km altitude, and the location of dip equator.

considerable extent within the longitudinal region of 67°E–81°E that are covered by our imager field of view (FOV). From the magnetic latitudes, apex altitudes over the dip equator are calculated according to *Chapagain et al.* [2012], assuming a fixed height of 250 km for OI 630 nm emission. In this calculation, it is assumed that the geomagnetic field lines are dipolar in nature. Thus, when airglow depletions corresponding to the EPBs are captured in the images, the approximate apex altitudes reached by them over the dip equator are obtained. Occasionally, poleward extension of the EPBs corresponding to the growth of the EPBs to higher apex altitudes or equatorward collapse representing shrinking of the EPBs toward lower apex altitudes is observed. Since we have calculated apex altitudes for each of the latitude in the airglow image, the extent of growth or collapse can be estimated from the two-dimensional images. Based on the difference in the apex altitudes reached by the EPBs and the time difference between the images, their rise velocities are also calculated. Here we discuss the importance and implications of the shrinking of the EPBs.

Simultaneous bottomside ionospheric parameters measured by Canadian Advanced Digital Ionosonde from dip equatorial site Tirunelveli (8.7°N, 77.8°E geographic; 1.1°N dip latitude) in the same longitudinal sector are also analyzed [*Narayanan et al.*, 2014]. The base height of the bottomside *F* region (*h'F*) is extracted from the ionograms that are usually spaced at 15 min time intervals. From the extracted base heights, vertical drifts are calculated as $V_D = d(h'F)/dt$. Also, the duration of equatorial spread *F* in the ionograms is noticed for comparison with the occurrence of EPBs in the images. Though the ionosonde observations are made at 77.8°E longitude, we assume that the measured parameters represent the background ionospheric behavior in the dip latitude region within the longitudinal range covered by the imager field of view (FOV). The schematic of imaging location, area covered by FOV at 250 km altitude, location of ionosonde observations, and the position of magnetic equator are shown in Figure 1.

3. Results

Figure 2 shows a set of all-sky images acquired on the night of 4 January 2008. The axis on the rightside of the images shows the apex altitudes over the dip equator corresponding to the geographic latitudes shown on the left axis. The bottom axis shows the longitudes, while the top axis indicates the local time at the respective longitudes during time of observation of the image. A total of five EPBs are shown in the images, wherein the fifth EPB is relatively larger in size. Figure 3 (bottom) shows the time variation of base height of *F* region ionosphere (*h'F*), and Figure 3 (top) shows the vertical drifts estimated from the base heights. The red line in the Figure 3 (bottom)indicates the duration of observation of ESF. The blue dots in the Figure 3 (top) represent the estimated rise speed of EPBs obtained from the images whose axis is given in the rightside of the plot.

Before 23:00 IST, the growth of first and third EPBs was noticed in the images (not shown) and the rise speeds measured are around 65 m/s (see Figure 3). Initially, the first EPB started shrinking, while the third EPB was still growing (see Figure 2, top left and middle). Afterward, all the EPBs were seen to decrease in the extent of their apex altitude as revealed in Figure 2. The shrinking speeds of the third and fourth EPBs estimated from images are around 50 m/s. At a later time, the fifth EPB was seen to collapse at a relatively faster rate of

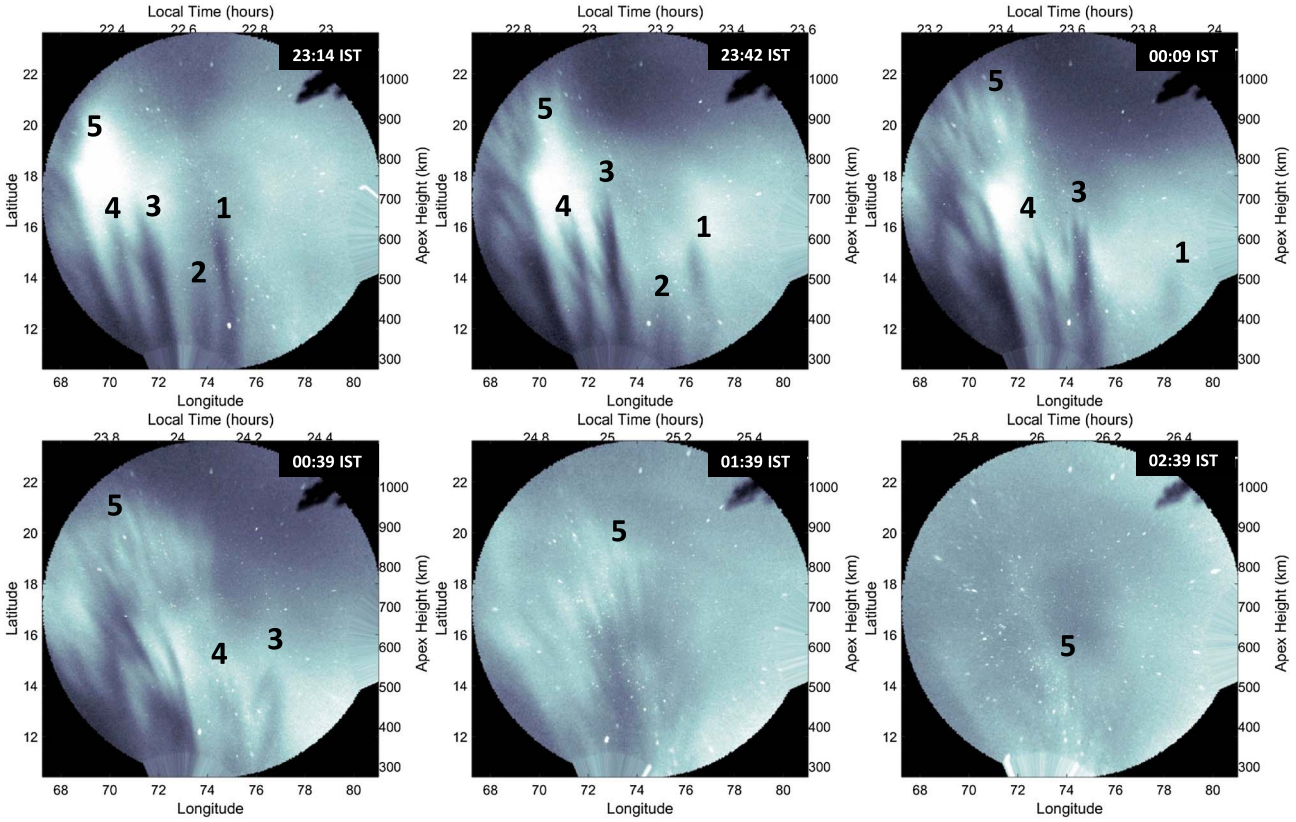

Figure 2. OI 630 nm airglow images obtained on the night of 4 January 2008 from Panhala. Consecutive EPBs are numbered. The geographic latitudes and longitudes covered in the image are given respectively in left and bottom axis, while apex altitude over dip equator and local time corresponding to the longitudes are given in right and top axis, respectively.

65 m/s as revealed by blue dots in Figure 3. It may be noted that from the third EPB onward, clear finger-like structures were seen to evolve at the edges of the EPBs, and when the EPBs shrink in apex altitude, those features were still present, and they also moved downward. However, some of the shortest finger-like structures evolved into more diffuse features with time. The downward movement of the branches and finger-like

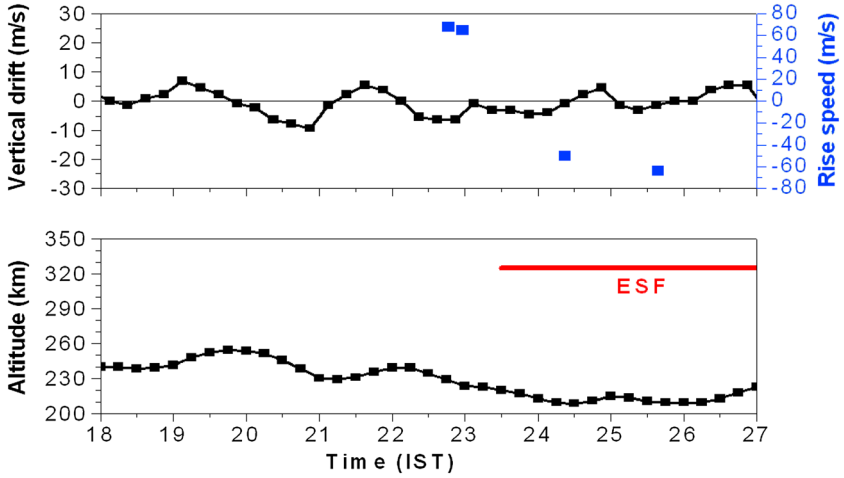

Figure 3. Ionospheric conditions over dip equator on 4 January 2008. (bottom) The variation of base height of *F* region ionosphere along with the duration of ESF in ionograms marked by red line. The black curve shows (top) the bottomside vertical drifts estimated from the altitude variation of base height, and the blue dots indicate the estimated rise or shrink speeds of EPBs measured from images.

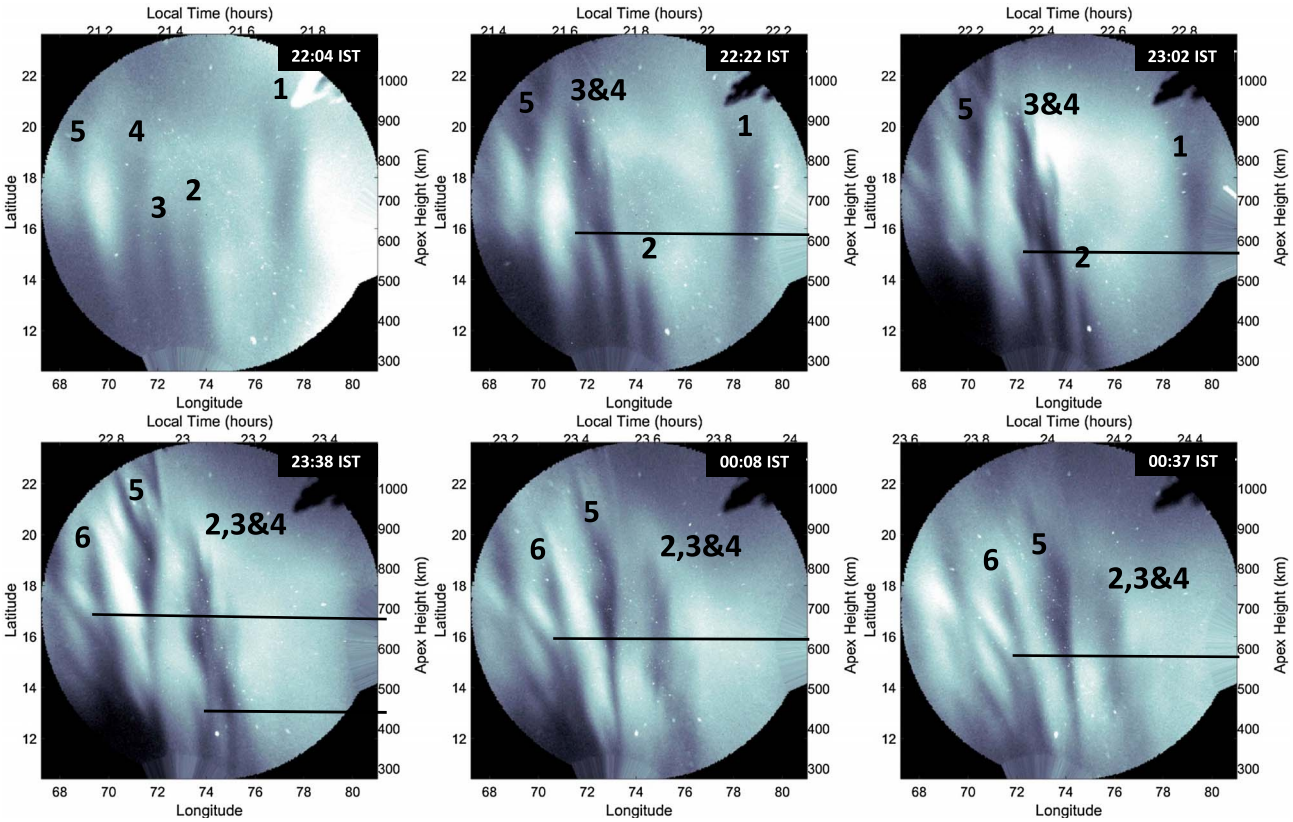

Figure 4. OI 630 nm airglow images obtained on the night of 6 January 2008 from Panhala. Consecutive EPBs are numbered. Two branches in different EPBs are marked with a line to indicate their descend in apex altitude.

structures implies that the shrinking observed is not due to the disappearance of a part of the bubbles in their topmost region. If the topmost part of the EPBs were disappearing the finger-like features are expected to disappear instead of moving down. From Figure 2 (bottom) it may be noticed that the fifth EPB shrank by about 400 km extent within 2 h. By about 03:30 IST, EPB signatures were totally vanished from the images. Nevertheless, the contrast of the EPB features were seen to decrease with time probably due to the reduction in the background plasma density in airglow emission heights during later hours of the night.

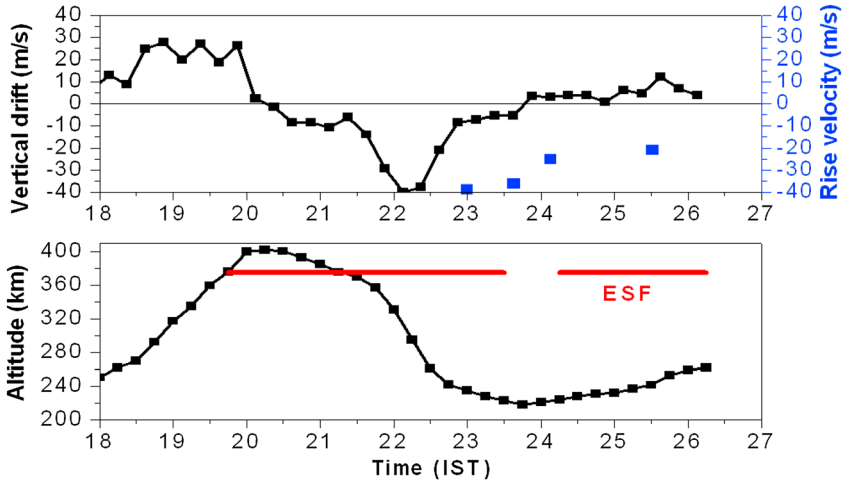

Figure 5. Same as Figure 3 but for 6 January 2008.

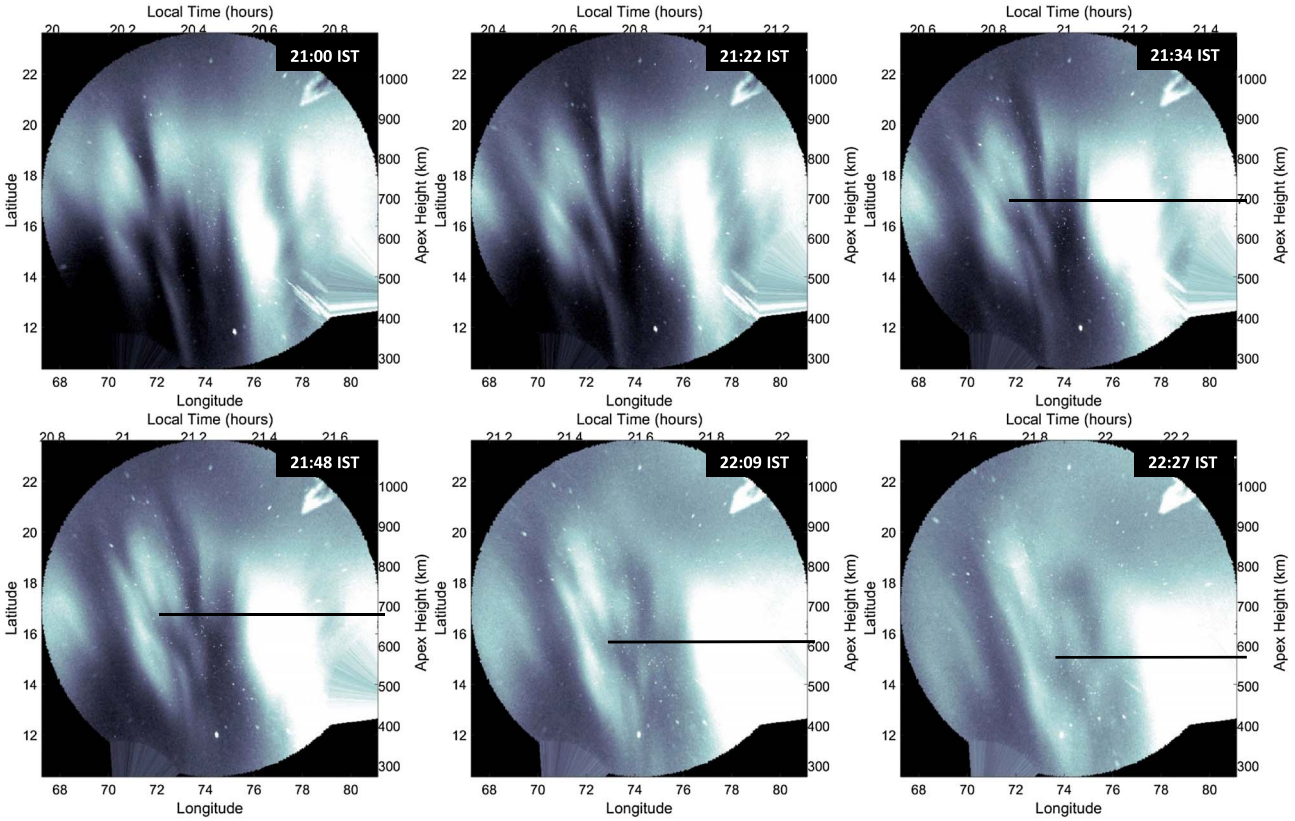

Figure 6. OI 630 nm airglow images obtained on the night of 3 February 2008 from Panhala. A branch that is descending along with the whole EPB is marked with a line.

From the ionosonde measurements it may be seen that the measured bottomside drifts are lesser compared to the observed shrinking speed of the EPBs. However, it should be noted that the observed collapse of the EPBs is happening at higher altitudes over the dip equator, and probably, downward plasma drift at those altitudes might be different from those on the bottomside. Earlier works show evidence for such differential drifts between different altitudes over the dip equator [*Pingree and Fejer*, 1987; *Fejer et al.*, 2014]. Comparing Figures 2 and 3, it may be noted that ESF signatures in ionograms are recorded as the EPBs arrive at locations close to the longitude of the ionosonde around 23:30 IST. Thus, the ESF recorded in the ionosonde did not originate overhead as revealed by the airglow images.

Figure 4 shows all-sky images acquired on the night of 6 January 2008. Figure 5 shows corresponding ionospheric measurements in the same format of Figure 3. In the airglow images six consecutive EPBs are numbered. With time, the third and fourth EPBs merged as they grew. So their growth speed could not be obtained. The merging will be separately discussed in another paper. Here the focus is on the shrinking aspect of EPBs. On this night the EPBs were seen to shrink after 22:00 IST. It may be seen that initially, the second EPB shrank when the third and fourth were growing and merging (compare Figure 4, top left and middle). It is important to note that one EPB shrank when the adjacent EPB separated by less than 100 km distance was growing. This indicates that the observed shrinking is not entirely due to something that happens on a larger scale in the background ionosphere. Afterward, the merged EPBs also started to collapse along with further merging with the second EPB. Those EPBs that followed the merging EPBs were seen to shrink as well. The lines drawn in the images represent the location of selected branching features in the merged EPB numbered as 3 and 4 and another branching feature clearly seen at the sixth EPB. It may be seen that the branching regions also move downward along with the downward motion of overall EPBs. Once again, the implication is that the shrinking is not an apparent feature due to disappearance of top portion of EPBs.

At the same time, Figure 5 shows that after about 22:30 IST, the variation in the base height of ionosphere was within 10 km indicating near zero vertical drifts. Thus, the observed speed of shrinking is different from the bottomside drifts measured. It may be noted that spread *F* was observed in ionograms on this night in

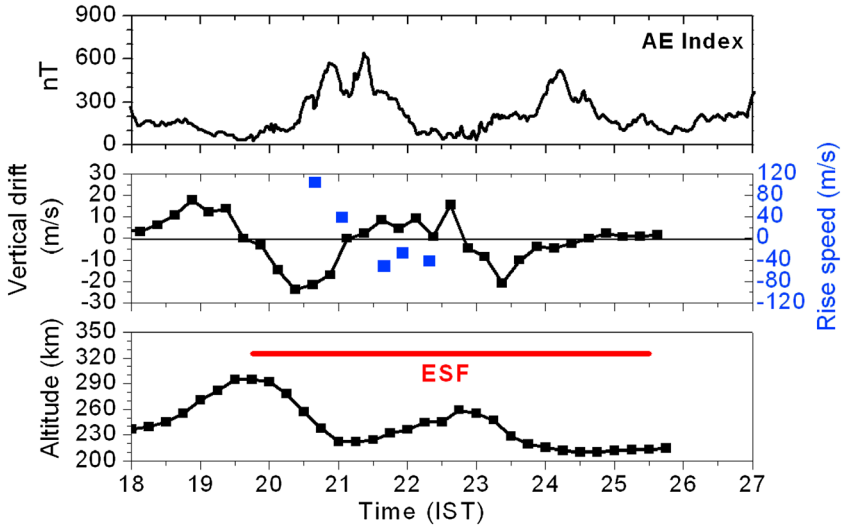

Figure 7. The bottom and middle plots are similar to the bottom and top plots in Figure 3 but for 3 February 2008. The top plot here shows *AE* index.

concurrence with observation of EPBs around 77.8°E longitude in the airglow images. Particularly, no spread *F* signatures were present between 23:30 and 00:00 IST when there are no EPBs close to the 77.8°E longitude. During that period the region in between EPBs 1 and 2 are traversing the overhead sky of ionosonde location (see Figure 4, bottom left).

Figure 6 shows EPBs observed on 3 February 2008. The time of EPB observations on this night coincides with the occurrence of an auroral substorm. In Figure 7, we have plotted three panels to show the *AE* indices at the top, vertical drifts and plasma bubble rise velocities at the middle and base height of ionosphere and the presence of ESF at the bottom, respectively. Figure 7 (middle and bottom) are similar to Figures 3 and 5. From Figure 7, it might be noticed that the equatorial ionospheric base height increases during the substorm recovery phase from about 21:15 IST. Earlier studies indicate that after about 21:00 LT in the months of November to February, the prompt penetration over shielding (under shielding) electric field is directed eastward (westward) [*Fejer and Scherliess*, 1995; *Tsunomura*, 1999; *Fejer et al.*, 2008]. Hence, the coincident rise of equatorial bottomside ionosphere appears to be the effect of prompt penetration over shielding electric fields that are eastward.

On this night both growth and shrinking of the EPBs were noticed (see Figure 6). The growth may be noticed as poleward development of EPBs between Figure 6 (top left and middle). After around 21:30 IST, the EPBs started to shrink with estimated speeds varying between 30 and 50 m/s. From Figure 7, it can be seen that the bottomside ionosphere was drifting upward while the EPBs were shrinking. This observation clearly shows that the observed apex altitude decrease of EPBs is not similar to the background bottomside ionospheric drift. Therefore, the decrease in the maximum apex altitude of EPBs is certainly not due to the overall downward motion of the ionosphere. Another implication of this observation is that the drifts might be different in different altitudes in equatorial ionosphere. On this night also, there is a good correlation between occurrence of EPBs in images and ESF in ionograms. In addition, Figure 6 reveals a reduction in the contrast of the EPBs with passage of time, similar to Figure 2.

Figures 8 and 9, respectively, show the imager observations from Panhala and ionosonde measurements from Tirunelveli on the night of 4 February 2008. On this night three EPBs were observed to enter the FOV of imager after 00:30 IST. No growth was observed on this night. The EPBs were drifting eastward with approximate zonal drift speed of 55 m/s and shrinking in their altitudinal extent. The zonal distance moved by an EPB is estimated from unwarped airglow images, and based on the time separation between the images, zonal drift speed is calculated. In Figure 8, a line is drawn to a branch in third EPB, which clearly indicates the downward movement of EPBs.

On this night, the bottomside drifts over the dip equator are weakly upward during the time of shrinking. It is interesting to note that there was no ESF trace in the ionograms on this night. The last OI 630 nm image observed on this night was at 02:26 IST. By comparing the locations of EPBs (around 74°E longitude) at that

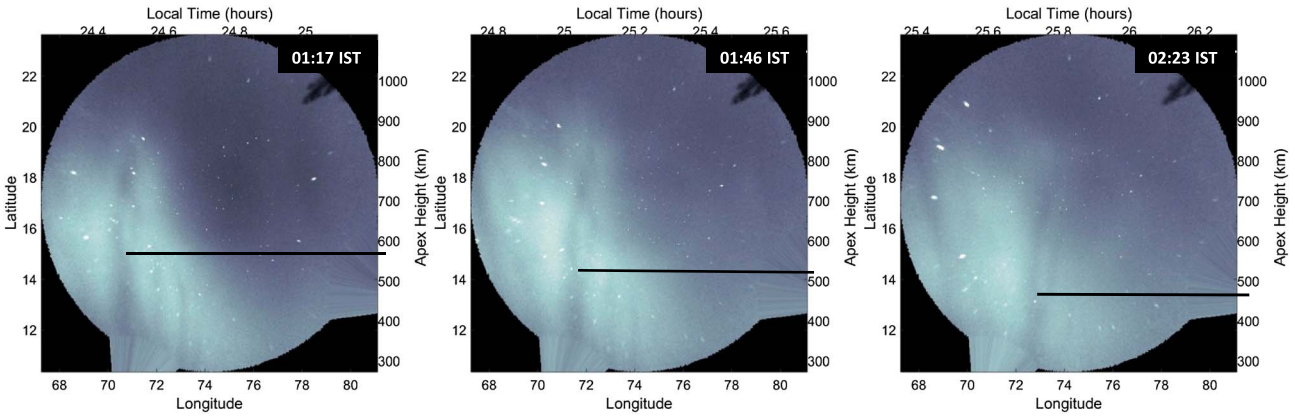

Figure 8. OI 630 nm airglow images obtained on the night of 4 February 2008 from Panhala. A line indicates the descending motion of a branch in one of the EPBs similar to Figures 4 and 6.

time and assuming that they drift eastward at the fixed rate of 55 m/s, those features are expected to arrive at the location of ionosonde only by about 04:00 IST. Around that time the ionospheric density measured by the ionosonde decreased below the sensitivity of the instrument. From Figure 9, it may be seen that there is a shrinking measurement around 21:30 IST. It corresponded to an EPB that is not shown here. That EPB was seen to shrink and soon disappeared before it reached 75°E longitude, and hence, no ESF was observed in ionosonde. Afterward, no EPBs were observed till 00:30 IST.

4. Discussion

Simulations done by *Krall et al.* [2010b] indicated that airglow signatures of the fossil bubbles might show some reduction in their topmost extent because plasma diffusing along the field lines from higher altitudes tend to fill the outermost regions soon after the growth of EPBs stop. However, note from Figures 2, 4, 6, and 8 that we are not observing disappearance at the top as the finger-like structures or branches in the EPBs also move downward in their apex altitudes (or latitudinal extent in images). As mentioned earlier, if the reduction at the top of the EPBs (equivalently at the poleward edge of EPBs) in images is caused by partial refilling, the movement of such branches is not expected. Rather, those fingers or branches should disappear. Furthermore, we observe the shrinking to continue till the EPBs disappear or move out of the imager FOV. Therefore, it is clear that the shrinking of EPBs is not an apparent effect observed in all-sky airglow images but a real aspect associated with collapse of whole EPBs.

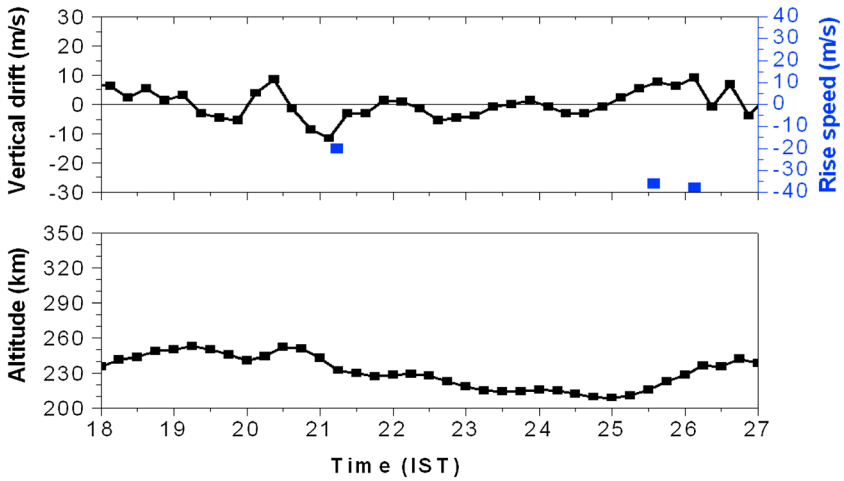

Figure 9. Same as Figure 3 but for 4 January 2008.

The cases discussed herein do not appear similar to those reported by *Otsuka et al.* [2012] and *Shiokawa et al.* [2015], wherein interaction with TIDs caused disappearance of EPBs. The scale sizes of TIDs and their longitudinal extents are larger than few hundred kilometers. As noted in Figure 4, our observations indicate that there are occasions when one EPB is shrinking while the adjacent EPB located within 100 km distance is growing. Figure 2 also showed that initially one EPB was shrinking while the others were not shrinking. Such observations indicate that it is unlikely for the observed shrinking phenomenon to be linked to the larger-scale size variations occurring in the bottomside ionosphere. Further, in the earlier reports of *Otsuka et al.* [2012] and *Shiokawa et al.* [2015], the disappearance of EPBs or substantial weakening occurred at shorter time scales (within an hour). Whereas the observations presented here do not reveal sudden weakening or disappearance of EPBs. Instead, they show a gradual reduction in the topmost altitudes reached by the EPBs.

It may be argued that the shrinking observed is a consequence of overall downward motion of the ionosphere at nighttimes. In order to test the possibility we compared the bottomside drifts with the shrinking speeds estimated. Generally, the magnitude of bottomside drifts were different from the estimated shrinking speeds. Particularly, during disturbed periods of 3 February 2008, we found that the bottomside drifts are certainly different from the shrinking speed of EPBs (Figure 7). This observation indicates at the possibility of altitudinal variations in ionospheric electric fields and vertical drifts. In such a case, though the bottomside ionosphere experience upward drifts, topside ionosphere might be drifting downward.

The vertical drifts in the equatorial ionosphere at any altitude is dependent on the zonal electric field in that altitude. Since the geomagnetic field lines are equipotentials, the topside equatorial ionosphere is interconnected to the off-equatorial low-latitude electric fields in both the hemispheres. Though the nocturnal zonal electric field is expected to be westward directed, the strength might differ with latitude and it may be reflected as altitudinal variation over equatorial topside ionosphere. In such a case, the vertical drifts in equatorial region will vary with altitudes as well. Especially during geomagnetically disturbed conditions, the penetration of polar electric fields primarily occur in the bottomside of the equatorial ionosphere where Pedersen conductivities are higher [*Kikuchi and Araki*, 1979; *Kikuchi and Hashimoto*, 2016]. Therefore, the events like that on 3 February 2008 (Figures 6 and 7) are possible wherein the bottomside ionosphere is being lifted up due to penetration electric fields while the topside drifts are downward as they are connected to nocturnal westward fields in off-equatorial latitudes through geomagnetic field lines.

An important aspect to be noted is that the collapse of whole EPBs as shown here is possible only if the plasma outside the EPB in topmost regions could push the EPBs downward. Equivalently, this indicates that the field-line-integrated plasma concentration above the bubble is not equal to that within the bubble but is greater than the plasma density within the bubble. In such a case, based on the nocturnal westward electric fields mapped to those higher altitudes, the EPBs might be pushed downward through the $E \times B$ drift. The observed shrinking speeds of a few tens of m/s might be caused by the nighttime westward electric fields felt at topside ionospheric altitudes. Jicamarca measurements show that downward drifts in the topside equatorial ionosphere reaches few tens of m/s [*Fejer et al.*, 1991, 2014]. Therefore, it is probable that the background topside downward drift might be equal to the observed shrink speeds.

If the EPBs have grown until their field-line-integrated ion mass densities are equal to that of the surroundings, the shrinking will not occur unless the eastward drift of EPBs takes them to a different longitudinal region where the field-line-integrated ion mass densities are higher above the EPBs. On the other hand, if the polarization eastward electric field within the EPBs decay before the EPBs grow to the full extent (i.e., till filed-line-integrated plasma densities within and outside are equal), it is likely that the field-line-integrated plasma density above the bubbles are greater. In such a case the EPBs will be pushed downward and can be seen as shrinking EPBs. However, the cause for the decay of the polarization electric field within EPB is not clear now. It might be possible for the polarization electric fields to be shorted out by the presence of sporadic E layers in the off equatorial region. Such layers might favor current flow which might remove the polarization electric fields within the EPBs. There may be unexplored mechanisms that might be acting in order to reduce the polarization electric fields within the EPBs. Any role of winds, both horizontal and vertical, needs to be explored further. At present it is unclear how winds might cause shrinking of EPBs.

As already mentioned the importance of the current finding is that it provides a mechanism by which the EPBs can decay before sunrise. For example, assume that an EPB has grown to 1000 km altitude and stopped rising due to decay of the polarization electric field. Taking an approximate downward drift of 40 m/s in

concurrence with the measured values reported herein, it will approximately shrink at a rate of 145 km/h. If the shrinking is started by about 23:00 LT, by about 04:30 LT, well before sunrise, the EPB might be reduced to apex altitudes of 200 km in the bottomside *F* region where it becomes extinct. In this way a reasonable number of the EPBs reaching higher altitudes over the dip equator might decay in the nighttime itself. Or at least they might be brought down to lower apex altitudes before sunrise so that they can be easily refilled within few minutes after the *F* region sunrise. Only those EPBs whose polarization fields sustain till they grow to the maximum possible extent wherein the plasma densities within and outside the EPBs are equal might be required to stay till sunrise hours for refilling. Even in those cases, downward push might occur if their zonal drifts bring them to longitudinal regions in which the field-line-integrated plasma density above the EPB is higher than that within the EPB. This might explain the scarcity of ESF observations in the morning hours in spite of a large number of reports that identify scintillations, ESF, and plasma depletions in the EIA crest region.

5. Concluding Remarks

In this work, for the first time we show the cases in which the EPBs were seen to shrink in their latitudinal extent in airglow images, which correspond to a reduction in their apex altitudes over the dip equator. We have shown that the observations are not apparent effect observed in airglow. The downward movement of EPBs is not matching with the bottmoside drifts of the equatorial *F* region ionosphere. We have discussed the importance of these observations. Such collapse of EPBs provides a way for them to decay completely or at least to descend to lower apex altitudes wherein refilling after sunrise will be much faster. These observations appear to highlight a decay phase of EPBs that is not noticed earlier. We expect to carry out further studies of such events which might reveal better insights in the decay of EPBs.

Acknowledgments
We thank P.T. Patil for his assistance in conducting the campaigns at Panhala and S. Sripathi for his role in maintaining the ionosonde and preserving the data. The data used in this work are collected by Indian Institute of Geomagnetism, and the contact person for data requests is S. Gurubaran. This work is primarily supported through the INSPIRE Faculty award of V.L.N. by Department of Science and Technology, Government of India (grant DST/INSPIRE/04/2014/001636). This work is also supported by JSPS KAKENHI grant 15H05815 and JSPS Core-to-Core Program, B. Asia-Africa Science Platforms. A part of this work was carried out under the joint research program of the Institute for Space-Earth Environmental Research, Nagoya University.

References

Abadi, P., S. Saito, and W. Srigutomo (2014), Low-latitude scintillation occurrences around the equatorial anomaly crest over Indonesia, *Ann. Geophys.*, *32*, 7–17, doi:10.5194/angeo-32-7-2014.

Abdu, M. A., R. T. de Medeiros, J. A. Bittencourt, and I. S. Batista (1983), Vertical ionization drift velocities and range type spread *F* in the evening equatorial ionosphere, *J. Geophys. Res.*, *88*, 399–402, doi:10.1029/JA088iA01p00399.

Abdu, M. A., E. A. Kherani, I. S. Batista, E. R. de Paula, D. C. Fritts, and J. H. A. Sobral (2009), Gravity wave initiation of equatorial spread *F*/plasma bubble irregularities based on observational data from the SpreadFEx campaign, *Ann. Geophys.*, *27*, 2607–2622, doi:10.5194/angeo-27-2607-2009.

Abdu, M. A., J. R. de Souza, E. A. Kherani, I. S. Batista, J. W. MacDougall, and J. H. A. Sobral (2015), Wave structure and polarization electric field development in the bottomside *F* layer leading to postsunset equatorial spread *F*, *J. Geophys. Res. Space Physics*, *120*, 6930–6940, doi:10.1002/2015JA021235.

Aggson, T. L., N. C. Maynard, W. B. Hanson, and J. L. Saba (1992), Electric field observations of equatorial bubbles, *J. Geophys. Res.*, *97*, 2997–3009, doi:10.1029/90JA02356.

Aggson, T. L., H. Laakso, N. C. Maynard, and R. F. Pfaff (1996), In situ observations of bifurcation of equatorial ionospheric plasma depletions, *J. Geophys. Res.*, *101*, 5125–5132, doi:10.1029/95JA03837.

Basu, S., S. Basu, J. Aarons, J. P. McClure, and M. D. Cousins (1978), On the coexistence of kilometer- and meter-scale irregularities in the nighttime equatorial *F* region, *J. Geophys. Res.*, *83*, 4219–4226, doi:10.1029/JA083iA09p04219.

Bhattacharyya, A., B. Kakad, S. Sripathi, K. Jeeva, and K. U. Nair (2014), Development of intermediate scale structure near the peak of the *F* region within an equatorial plasma bubble, *J. Geophys. Res. Space Physics*, *119*, 3066–3076, doi:10.1002/2013JA019619.

Burke, W. J., R. C. Sagalyn, R. G. Rastogi, M. Ahmed, F. J. Rich, D. E. Donatelli, and P. J. L. Wildman (1979), Postsunrise refilling of the low-latitude topside ionosphere, *J. Geophys. Res.*, *84*, 4201–4206, doi:10.1029/JA084iA08p04201.

Candido, C. M. N., I. S. Batista, F. Becker-Guedes, M. A. Abdu, J. H. A. Sobral, and H. Takahashi (2011), Spread *F* occurrence over a southern anomaly crest location in Brazil during June solstice of solar minimum activity, *J. Geophys. Res.*, *116*, A06316, doi:10.1029/2010JA016374.

Chapagain, N. P., M. J. Taylor, J. J. Makela, and T. M. Duly (2012), Equatorial plasma bubble zonal velocity using 630.0 nm airglow observations and plasma drift modeling over Ascension Island, *J. Geophys. Res.*, *117*, A06316, doi:10.1029/2012JA017750.

Chau, J. L., and R. F. Woodman (2001), Interferometric and dual beam observations of daytime spread-*F*-like irregularities over Jicamarca, *Geophys. Res. Lett.*, *28*, 3581–3584, doi:10.1029/2001GL013404.

Dyson, P. L. (1977), Topside irregularities in the equatorial ionosphere, *J. Atmos. Sol. Terr. Phys.*, *39*, 1269–1275, doi:10.1016/0021-9169(77)90036-8.

Fejer, B. G., and L. Scherliess (1995), Time dependent response of equatorial ionospheric electric fields to magnetospheric disturbances, *Geophys. Res. Lett.*, *22*, 851–854, doi:10.1029/95GL00390.

Fejer, B. G., E. R. de Paula, S. A. Gonzalez, and R. F. Woodman (1991), Average vertical and zonal *F* region plasma drifts over Jicamarca, *J. Geophys. Res.*, *96*, 13,901–13,906, doi:10.1029/91JA01171.

Fejer, B. G., L. Scherliess, and E. R. de Paula (1999), Effects of the vertical plasma drift velocity on the generation and evolution of equatorial spread *F*, *J. Geophys. Res.*, *104*, 19,859–19,869, doi:10.1029/1999JA900271.

Fejer, B. G., J. W. Jensen, and S.-Y. Su (2008), Seasonal and longitudinal dependence of equatorial disturbance vertical plasma drifts, *Geophys. Res. Lett.*, *35*, L20106, doi:10.1029/2008GL035584.

Fejer, B. G., D. Hui, J. L. Chau, and E. Kudeki (2014), Altitudinal dependence of evening equatorial *F* region vertical plasma drifts, *J. Geophys. Res. Space Physics*, *119*, 5877–5890, doi:10.1002/2014JA019949.

Finlay, C. C., et al. (2010), International Geomagnetic Reference Field: The eleventh generation, *Geophys. J. Int.*, *183*, 1216–1230, doi:10.1111/j.1365-246X.2010.04804.x.

Huang, C.-S., O. de La Beaujardiere, P. A. Roddy, D. E. Hunton, J. O. Ballenthin, and M. R. Hairston (2013), Long-lasting daytime equatorial plasma bubbles observed by the C/NOFS satellite, *J. Geophys. Res. Space Physics*, *118*, 2398–2408, doi:10.1002/jgra.50252.

Immel, T. J., H. U. Frey, S. B. Mende, and E. Sagawa (2004), Global observations of the zonal drift speed of equatorial ionospheric plasma bubbles, *Ann. Geophys.*, *22*, 3099–3107, doi:10.5194/angeo-22-3099-2004.

Jayachandran, B., N. Balan, P. B. Rao, J. H. Sastri, and G. J. Bailey (1993), HF Doppler and ionosonde observations of the onset conditions of equatorial spread F, *J. Geophys. Res.*, *98*, 13,741–13,750, doi:10.1029/93JA00302.

Kelley, M. C., M. F. Larsen, and C. LaHoz (1981), Gravity wave initiation of equatorial spread *F*: A case study, *J. Geophys. Res.*, *86*, 9087–9100, doi:10.1029/JA086iA11p09087.

Kikuchi, T., and K. K. Hashimoto (2016), Transmission of the electric fields to the low latitude ionosphere in the magnetosphere-ionosphere current circuit, *Geosci. Lett.*, *3*, 4, doi:10.1186/s40562-016-0035-6.

Kikuchi, T., and T. Araki (1979), Horizontal transmission of the polar electric field to the equator, *J. Atmos. Sol. Terr. Phys.*, *41*, 927–936, doi:10.1016/0021-9169(79)90094-1.

Krall, J., J. D. Huba, S. L. Ossakow, and G. Joyce (2010a), Why do equatorial ionospheric bubbles stop rising?, *Geophys. Res. Lett.*, *37*, L09105, doi:10.1029/2010GL043128.

Krall, J., J. D. Huba, S. L. Ossakow, and G. Joyce (2010b), Equatorial spread *F* fossil plumes, *Ann. Geophys.*, *28*, 2059–2069, doi:10.5194/angeo-28-2059-2010.

Laakso, H., T. L. Aggson, R. F. Pfaff, and W. B. Hanson (1994), Downdrafting plasma flow in equatorial bubbles, *J. Geophys. Res.*, *99*, 11,507–11,515, doi:10.1029/93JA03169.

Lee, C. C., F. D. Chu, W. S. Chen, J. Y. Liu, S.-Y. Su, Y. A. Liou, and S. B. Yu (2009), Spread F, GPS phase fluctuations, and plasma bubbles near the crest of equatorial ionization anomaly during solar maximum, *J. Geophys. Res.*, *114*, A08302, doi:10.1029/2009JA014195.

Lynn, K. J., Y. Otsuka, and K. Shiokawa (2011), Simultaneous observations at Darwin of equatorial bubbles by ionosonde-based range/time displays and airglow imaging, *Geophys Res Lett*, *38*, L23101, doi:10.1029/2011GL049856.

Makela, J. J. (2006), A review of imaging low-latitude ionospheric irregularity process, *J. Atmos. Sol. Terr. Phys.*, *68*, 1441–1458, doi:10.1016/j.jastp.2005.04.014.

Martinis, C., and M. Mendillo (2007), Equatorial spread *F*-related airglow depletions at Arecibo and conjugate observations, *J. Geophys. Res.*, *112*, A10310, doi:10.1029/2007/JA012403.

Martinis, C., J. Baumgardner, M. Mendillo, S.-Y. Su, and N. Aponte (2009), Brightening of 630.0 nm equatorial spread-*F* airglow depletions, *J. Geophys. Res.*, *114*, A06318, doi:10.1029/2008JA013931.

McClure, J. P., S. Singh, D. K. Bamgboye, F. S. Johnson, and H. Kil (1998), Occurrence of equatorial *F* region irregularities: Evidence for tropospheric seeding, *J. Geophys. Res.*, *103*, 29,119–29,135, doi:10.1029/98JA02749.

Mendillo, M., E. Zesta, S. Shodham, P. J. Sultan, R. Doe, Y. Sahai, and J. Baumgardner (2005), Observations and modeling of the coupled latitude-altitude patterns of equatorial plasma depletions, *J. Geophys. Res.*, *110*, A09303, doi:10.1029/2005JA011157.

Mukherjee, G. K. (2003), Studies of equatorial *F*-region depletions and dynamics using multiple wavelength nightglow imaging, *J. Atmos. Sol. Terr. Phys.*, *65*, 379–390, doi:10.1016/S1364-6826(02)00214-6.

Nade, D. P., A. K. Sharma, S. S. Nikte, P. T. Patil, R. N. Ghodpage, M. V. Rokade, S. Gurubaran, A. Taori, and Y. Sahai (2013), Zonal velocity of the equatorial plasma bubbles over Kolhapur, India, *Ann. Geophys.*, *31*, 2077–2084, doi:10.5194/angeo-31-2077-2013.

Nade, D. P., D. J. Shetti, A. K. Sharma, A. Taori, G. A. Chavan, P. T. Patil, R. N. Ghodpage, O. B. Gurav, and S. S. Nikte (2015), Geographical analysis of equatorial plasma bubbles by GPS and nightglow measurements, *Adv. Space Res.*, *56*, 1901–1910, doi:10.1016/j.asr.2015.03.030.

Narayanan, V. L., S. Gurubaran, and K. Emperumal (2009), Imaging observations of upper mesospheric nightglow emissions from Tirunelveli (8.7°N), *Indian J. Radio Space Phys.*, *38*, 150–158.

Narayanan, V. L., S. Gurubaran, K. Emperumal, and P. T. Patil (2011), Unusual optical observations of OI greenline during a geospace event on 1 February 2008, *J. Geophys. Res.*, *116*, A09315, doi:10.1029/2010JA016339.

Narayanan, V. L., A. Taori, A. K. Patra, K. Emperumal, and S. Gurubaran (2012), On the importance of wave-like structures in the occurrence of equatorial plasma bubbles: A case study, *J. Geophys. Res.*, *117*, A01306, doi:10.1029/2011JA017054.

Narayanan, V. L., S. Gurubaran, K. Emperumal, and P. T. Patil (2013), A study on the nighttime equatorward movement of ionization anomaly using thermospheric airglow imaging technique, *J. Atmos. Sol. Terr. Phys.*, *103*, 113–120, doi:10.1016/j.jastp.2013.03.028.

Narayanan, V. L., S. Sau, S. Gurubaran, K. Shiokawa, N. Balan, K. Emperumal, and S. Sripathi (2014), A statistical study of satellite traces and evolution of equatorial spread *F*, *Earth Planets Space*, *66*, 160, doi:10.1186/s40623-014-0160-4.

Otsuka, Y., K. Shiokawa, and T. Ogawa (2012), Disappearance of equatorial plasma bubble after interaction with mid-latitude medium-scale traveling ionospheric disturbance, *Geophys. Res. Lett.*, *39*, L14105, doi:10.1029/2012GL052286.

Patra, A. K., P. Srinivasulu, P. P. Chaitanya, M. D. Rao, and A. Jayaraman (2014), First results on low-latitude *E* and *F* region irregularities obtained using the Gadanki Ionospheric Radar Interferometer, *J. Geophys. Res. Space Physics*, *119*, 10,276–10,293, doi:10.1002/2014JA020604.

Pingree, J. E., and B. G. Fejer (1987), On the height variation of the equatorial *F* region vertical plasma drifts, *J. Geophys. Res.*, *92*, 4763–4766, doi:10.1029/JA092iA05p04763.

Rajesh, P. K., J. Y. Liu, H. S. S. Sinha, and S. B. Banerjee (2010), Appearance and extension of airglow depletions, *J. Geophys. Res.*, *115*, A08318, doi:10.1029/2009JA014952.

Rao, P. B., A. K. Patra, T. V. C. Sarma, B. V. Krishnamurthy, K. S. V. Subba Rao, and S. S. Hari (1997), Radar observations of updrafting and downdrafting plasma depletions associated with the equatorial spread *F*, *Radio Sci.*, *32*, 1215–1227, doi:10.1029/97RS00094.

Rino, C. L., R. T. Tsunoda, J. Petriceks, R. C. Livingston, M. C. Kelley, and K. D. Baker (1981), Simultaneous Rocket-borne beacon and in situ measurements of equatorial spread *F*—Intermediate wavelength results, *J. Geophys. Res.*, *86*, 2411–2420, doi:10.1029/JA086iA04p02411.

Rohrbaugh, R. P., W. B. Hanson, B. A. Tinsley, B. L. Cragin, J. P. McClure, and A. L. Broadfoot (1989), Images of transequatorial bubbles based on field-aligned airglow observations from Haleakala in 1984–1986, *J. Geophys. Res.*, *94*, 6763–6770, doi:10.1029/JA094iA06p06763.

Saito, S., S. Fukao, M. Yamamoto, Y. Otsuka, and T. Maruyama (2008), Decay of 3-m-scale ionospheric irregularities associated with plasma bubble observed with the equatorial atmosphere radar, *J. Geophys. Res.*, *113*, A11318, doi:10.1029/2008JA013118.

Sekar, R., E. A. Kherani, P. B. Rao, and A. K. Patra (2001), Interaction of two long-wavelength modes in the nonlinear numerical simulation of equatorial spread F, *J. Geophys. Res.*, *106*, 24,765–24,775, doi:10.1029/2000JA000361.

Sharma, A. K., D. P. Nade, S. S. Nikte, P. T. Patil, R. N. Ghodpage, R. S. Vhatkar, M. V. Rokade, and S. Gurubaran (2014), Occurrence of equatorial plasma bubbles over Kolhapur, *Adv. Space Res.*, *54*, 435–442, doi:10.1016/j.asr.2013.07.018.

Shiokawa, K., Y. Otsuka, K. J. W. Lynn, P. Wilkinson, and T. Tsugawa (2015), Airglow-imaging observation of plasma bubble disappearance at geomagnetically conjugate points, *Earth Planets Space*, *67*, 43, doi:10.1186/s40623-015-0202-6.

Sidorova, L. N. (2007), Plasma bubble phenomenon in the topside ionosphere, *Adv. Space Res.*, *39*, 1284–1291, doi:10.1016/j.asr.2007.03.067.

Sidorova, L. N., and S. V. Filippov (2014), Plasma bubbles in the topside ionosphere: Estimations of the survival possibility, *J. Atmos. Sol. Terr. Phys.*, *119*, 35–41, doi:10.1016/j.jastp.2014.06.013.

Sinha, H. S. S., and S. Raizada (2000), Some new features of ionospheric plasma depletions over the Indian zone using all sky optical imaging, *Earth Planets Space*, *52*, 549–559, doi:10.1186/BF03351662.

Sultan, P. J. (1996), Linear theory and modeling of the Rayleigh-Taylor instability leading to the occurrence of equatorial spread *F*, *J. Geophys. Res.*, *101*, 26,875–26,891, doi:10.1029/96JA00682.

Taori, A., and A. Sindhya (2014), Measurements of equatorial plasma depletion velocity using 630 nm airglow imaging over a low-latitude Indian station, *J. Geophys. Res. Space Physics*, *119*, 396–401, doi:10.1002/2013JA019465.

Tsunomura, S. (1999), Numerical analysis of global ionospheric current system including the effect of equatorial enhancement, *Ann. Geophys.*, *17*, 692–706, doi:10.1007/s00585-999-0692-2.

Watanabe, S., and H. Oya (1986), Occurrence characteristics of low latitude ionosphere irregularities observed by the impedance probe on board the Hinotori Satellite, *J. Geomagn. Geoelectr.*, *38*, 125–149, doi:10.5636/jgg.38.125.

Woodman, R. F., and C. La Hoz (1976), Radar observations of *F* region equatorial irregularities, *J. Geophys. Res.*, *31*, 5447–5466, doi:10.1029/JA081i031p05447.

Woodman, R. F., J. E. Pingree, and W. E. Swartz (1985), Spread-*F*-like irregularities observed by the Jicamarca radar during the day-time, *J. Atmos. Sol. Terr. Phys.*, *47*, 867–874, doi:10.1016/0021-9169(85)90061-3.